Materials Chemistry and Physics 253 (2020) 123427

Contents lists available at ScienceDirect

Materials Chemistry and Physics

journal homepage: www.elsevier.com/locate/matchemphys

High thermoelectric performance of *p*-type $Bi_{0.5}Sb_{1.5}Te_3$ films on flexible substrate

T. Parashchuk [a,*], O. Kostyuk [b], L. Nykyruy [b], Z. Dashevsky [c]

[a] The Lukasiewicz Research Network – Krakow Institute of Technology, Krakow, 30-011, Poland
[b] Vasyl Stefanyk Precarpathian National University, Ivano-Frankivsk, 76018, Ukraine
[c] Department of Materials Engineering, Ben-Gurion University, Beer-Sheva, 84105, Israel

HIGHLIGHTS

- A technology for fabrication of *p*-$Bi_{0.5}Sb_{1.5}Te_3$ films has been developed.
- The transport properties have been studied over the entire temperature range.
- The density of states effective mass and carrier scattering mechanism were estimated.
- The highest reported values of the ZT and PF for a flexible film was obtained.

ARTICLE INFO

Keywords:
Thin film
$Bi_{0.5}Sb_{1.5}Te_3$ semiconductor
Thermoelectric properties
Flexible thermoelectric

ABSTRACT

Bi_2Te_3-based compounds are excellent candidates for the low-temperature thermoelectric application. In the present work, a technology for fabrication of *p*-$Bi_{0.5}Sb_{1.5}Te_3$ films with high thermoelectric efficiency on a thin flexible polyimide substrate has been developed. The preparation of films was carried out by a flash evaporation method. A systematic study of the transport properties (Hall coefficient, Seebeck coefficient, electrical conductivity, transverse Nernst coefficient) over the entire temperature range of 80–400 K for *p*-$Bi_{0.5}Sb_{1.5}Te_3$ films has been performed. The power factor (PF) for the $Bi_{0.5}Sb_{1.5}Te_3$ (doped by 0.5 wt % Te) film reaches the value of ~30.4 μW $cm^{-1}K^{-2}$, which is among the highest values of the PF reported in the literature to date for a film on a flexible polyimide (amorphous) substrate. The measured thermal diffusivity along the film allowed us to accurately estimate the figure of merit *Z* for *p*-$Bi_{0.5}Sb_{1.5}Te_3$ films considering the anisotropic effect of Bi_2Te_3-based materials. A significant enhancement of *Z* up to ~3.0×10^{-3} K has been obtained for these films, which is state-of-the-art even compared to bulk materials. This research can provide insight into the fabrication of *p*-type branch of the Film Thermoelectric Modules (FTEM), which could be a candidate for application in micro-scale thermoelectric generators.

1. Introduction

Recently, the requirements for microelectronic applications with a power of few microwatts at relatively high voltage for the operation of small electric devices and systems have been increasing [1,2]. A film thermoelectric generator (FTEG) could be the ideal on-board power supply for such purposes. It can directly produce small electrical power from thermal energy. The output power of such microdevices is in the range from 100 nW to 10 mW, which is a typical range of power generated from the surface of a human body [3–6]. For obtaining the FTEG with acceptable application characteristics, materials with high thermoelectric performance are essential.

The efficiency of converting heat into electricity is determined by the thermoelectric figure of merit *Z*:

$$Z = \frac{S^2\sigma}{\kappa}, \quad (1)$$

where *S* is the Seebeck coefficient, σ, and κ are the electrical and thermal conductivity, respectively.

Therefore, an effective thermoelectric material should meet the following criteria [7]:

Semiconductor material (elemental, compound, alloy, composite,

* Corresponding author.
E-mail address: taras.parashchuk@kit.lukasiewicz.gov.pl (T. Parashchuk).

https://doi.org/10.1016/j.matchemphys.2020.123427
Received 6 December 2019; Received in revised form 29 May 2020; Accepted 14 June 2020
Available online 17 June 2020

multilayer, superlattice, low-dimensional structure) should preferably consist of heavy atoms. This will result in a low frequency of thermal vibrations of lattice and a significant decrease in lattice thermal conductivity κ_L.

The semiconductor material should have high dielectric constant $\varepsilon > 100$, which reduces the scattering of charge carriers by impurity ions and the low effective mass of major charge carriers (electrons for *n*-type and heavy holes for *p*-type). These two criteria provide high mobility of charge carriers μ.

Note that the high dielectric constant ε leads to a decrease in the ionization energy of the impurity atoms (which is practically approaching zero). As a result, the energy level of impurity merges with the conduction or valence band, and the concentration of electrons in the conduction band of *n*-type material or the concentration of heavy holes in the valence band of *p*-type material becomes constant (similar to metallic conductivity) and equal to dopant concentration in the temperature range from 0 K to the onset of intrinsic conductivity.

Semiconductor materials should have a high degeneracy of the conduction band for *n*-type and the same valence band degeneracy for *p*-type. In this case, the concentration of charge carriers increases significantly without changing the Fermi level E_F position, since it is directly proportional to the number of ellipsoids and, therefore, the electrical conductivity shows a significant growth as well.

The solubility limit of doping elements in a semiconductor shall be high, ensuring the achievement of high concentrations of charge carriers $n(p) > 10^{19}$ cm^{-3}. Consequently, the optimal Fermi level energy E_F [$(E_C - E_F) \sim 0$ eV for *n*-type and $(E_V - E_F) \sim 0$ eV for *p*-type] and the maximum value of power factor $PF = S^2\sigma$ could be obtained.

Bandgap E_g of semiconductor in the operating temperature range of the thermoelectric material should be $E_g > 8k_0T$ to minimize the contribution of thermally generated minority charge carriers to the total electrical conductivity, leading to a decrease in thermoelectric efficiency.

Bi_2Te_3 and its alloys are commercialized as materials for thermoelectric refrigeration [8,9] and perfectly meet the above criteria. It is also the best material for use in thermoelectric generators at a moderate temperature of the heat source [8,9]. Bismuth, Antimony, and Telluride are among the heaviest elements of the periodic table, and chemical bonds between them are not particularly rigid. Consequently, the unit cells are large, therefore, the Brillouin zones and the wave vectors of phonons are small. This leads to a naturally low intrinsic lattice thermal conductivity, even in perfect crystals, where it is limited only by anharmonic phonon-phonon interactions [10]. The solid solution of $Bi_{0.5}Sb_{1.5}Te_3$ grown from melt with 2.5 at. % of tellurium excess has a maximum reported value of $ZT \sim 0.9$ for bulk samples [8]. Tellurium has been introduced into the compound to compensate the acceptor effect of antimony resulting from stoichiometry displacement.

According to the Fourier low, for a thin film with thickness d_f deposited on a substrate with thickness d_s, the ratio of heat flow Q_f/Q_s through the film and the substrate:

$$\frac{Q_f}{Q_s} \sim \frac{\kappa_f d_f}{\kappa_s d_s} \tag{2}$$

Here, κ_f and κ_s are the thermal conductivity of the film and the substrate, respectively. Obviously, for optimal thermoelectrical performance of the film, the film deposition substrate should have the lowest possible values of thermal conductivity κ_s and thickness d_s.

Until now, films from Bi_2Te_3-based alloys have been fabricated by co-evaporation, molecular beam epitaxy, magnetron sputtering, and pulsed laser deposition methods [11–15]. The structural and microstructural properties of thin films on different types of substrates are well established in literature [16–20]. However, a high value of the figure of merit *Z* for Bi_2Te_3-based films such as *Z* for bulk crystals ($Z \sim 3 \times 10^{-3}$ K^{-1}) [21–24] has not been achieved.

In this work, we show that an optimized film preparation process is tremendously important. For film preparation, an ultrathin polyimide substrate with a thickness of ~10 μm was used, aiming to minimize detrimental heat wastes. The benefits of the polyimide material as a substrate are its extremely low thermal conductivity (~3.5 Wcm^{-1}K^{-1}) and high flexibility properties. Optimized technological conditions, proper film, and substrate thicknesses with subsequent annealing make it possible to achieve a significant improvement in the thermoelectric properties of the developed flexible *p*-$Bi_{0.5}Sb_{1.5}Te_3$ films, which are state-of-the-art even in comparison with bulk materials.

2. Experimental procedure

Synthesis of $Bi_{0.5}Sb_{1.5}Te_3$-based materials was carried out by direct melting of components for 10 h at 1073 K in sealed quartz ampoules evacuated to a residual pressure of 10^{-5} mbar. Each ampoule was then taken from the furnace and quenched in cold water. High purity components were used for the synthesis. The obtained ingots were crushed into fine powders by ball milling in an argon atmosphere. The preparation of $Bi_{0.5}Sb_{1.5}Te_3$ films with higher hole concentration was carried out using over stochiometric Pb (0.5–1.0 wt %) due to the acceptor effect of Pb at Bi_2Te_3-based compounds [8]. Lower concentration of the $Bi_{0.5}Sb_{1.5}Te_3$ composition was obtained by introducing over stochiometric Te (0.5–1 wt. %), which relates to the compensation effect of metal vacancies [8].

The *p*-type $Bi_{0.5}Sb_{1.5}Te_3$ thin films were deposited using flash evaporation technology, which was first developed by Z. Dashevsky for Bi_2Te_3 compounds [25]. The scheme as well as the operating principle of a typical flash evaporation apparatus is shown in the Appendix. The temperature of the substrate for film preparation was $T_s = 523$ K; evaporation velocity was $v_e = 0.1$ μm/min. After the evaporation process, all films were annealed in the same evaporation chamber at $T_t = 623$ K for 0.5 h in a pure argon atmosphere at pressure $p = 0.9$ atm.

The structural analyses of the films was studied using X-ray diffractometer STOE STADI P (by STOE &Cie GmbH, Germany) according to the modified Guinier geometry scheme using the transmission mode (CuKα_1-radiation, concave Ge-monochromator (111) of the Johann type; 2θ/ω-scan, angle interval $10.000^\circ \le 2\theta \le 125.185^\circ$ with the step of scanning 0.015°; the scan time in step 100–230 s). The initial processing of experimental diffraction arrays was performed using PowderCell (version 2.4) software packages. SEM images were taken with Quanta 200 environmental scanning electron microscope (HRSEM) equipped with energy-dispersive X-ray spectroscopy.

For the investigation of the transport properties on thin films (Seebeck coefficient *S*, electrical conductivity σ, Hall coefficient R_H, and transverse Nernst coefficient *Q*) over a wide temperature range of 80–500 K, a unique measurement setup was used [26]. The measurement of Hall and transverse Nernst effects were carried out in permanent magnetic fields up to 2 T. The results are averaged measurements in two directions of the electrical and magnetic fields. The accuracy of the temperature measurement was 0.1–0.2 K, and of the magnetic field ±3%. The uncertainty of the Seebeck coefficient and electrical conductivity measurements was 6%. The Hall effect was measured with an accuracy of 8% and the transverse Nernst effect – with an accuracy of 10%.

The study of heat transfer at *p*-$Bi_{0.5}Sb_{1.5}Te_3$ films on a flexible substrate is performed by the method of dynamic lattices [27]. It is based on the effect that the sample is excited by two mutually interfering laser beams. As a result, the samples are characterized by a dynamic diffraction lattice, and the kinetics of the diffraction signal can be analyzed. Finally, the value of thermal diffusivity α along the film was measured using this method. The uncertainty of the thermal diffusivity measurement was ~8%. A schematic view of the measurement set up, as well as detailed instruction, can be fined in Ref. [26,27]. The total thermal conductivity was calculated using the following formula:

$$\kappa = \alpha \rho c_p \ , \tag{3}$$

where ρ is the single crystal density, and c_p was estimated within the Dulong-Petit limit.

3. Results and discussion

3.1. Structural properties

Bi_2Te_3 and Sb_2Te_3 form a continuous solid solution. The structure of $Bi_{0.5}Sb_{1.5}Te_3$ consists of quintuple layers that are perpendicular to the *z*-axis in the hexagonal lattice, as shown in Fig. 1(a). Each quintet consists of five simple layers in which atoms interact with each other through covalent and ionic interactions. The quintuple layers are connected by weakly bonded Van der Waals forces. Such a complex structure with simultaneous introduction of Sb atoms in Bi positions leads to even higher dielectric constants in comparison with pristine Bi_2Te_3, which is vital for screening of ionized impurities and high thermoelectric performance of $Bi_{0.5}Sb_{1.5}Te_3$ solid solution [28,29]. The preferred orientations for Bi_2Te_3-based materials fabricated by the chemical-solution method or by physical vapor deposition are (001) and (015) [30,31].

The quality of investigated samples after synthesis and film preparation was checked using XRD analyses. In Fig. 1(b), a refinement of the $Bi_{0.5}Sb_{1.5}Te_3$ powder XRD experimental pattern using ICSD #617062 model confirms that the ingot after synthesis is single phase and without any impurities. The provided SEM-images with the EDS elemental analyses of the selected region for polished surface of as cast $Bi_{0.5}Sb_{1.5}Te_3$ ingot proved that the nominal concentration of elements is kept in the synthesized material (Fig. 1(c)). Fig. 1(d) shows XRD-patterns for the $Bi_{0.5}Sb_{1.5}Te_3$-based films on an amorphous thin polyimide substrate. The sharp reflections of XRD-patterns indicate the polycrystalline nature of the investigated samples. Similar to Ref. [32] (006) and (0015) are the dominant peaks when $Bi_{0.5}Sb_{1.5}Te_3$-based films were fabricated by the magnetron sputtering method on a tick polyimide substrate. This indicates the high quality of the sample texture [00*l*], i.e., all investigated films were oriented along the substrate plane with the direction perpendicular to the *z* axis of the $Bi_{0.5}Sb_{1.5}Te_3$ crystal lattice. The XRD reflections of the $Bi_{0.5}Sb_{1.5}Te_3$-based films belong to the $Bi_{0.5}Sb_{1.5}Te_3$ phase indicating a single-phase nature of the obtained specimens due to the small amounts of dopants used in the work.

Fig. 2 shows images of the secondary emission of the film surface for a representative $Bi_{1.5}Sb_{0.5}Te_3$ specimen. As can be seen from Fig. 2(a), excellent distribution of grain sizes as well as the absence of pores are observed for the investigated film. The surface of the crystallites is seen in the image with higher magnification in Fig. 2(b). The image with higher magnification also confirms the fine deposition of the material on the substrate and formation of plate-shaped grains, typical for layer structures of the studied solid solution. The estimated average grain size for $Bi_{1.5}Sb_{0.5}Te_3$ film on an amorphous substrate for the most common grains ranges from 600 to 800 nm, and the size of the largest grains does not exceed ~3 μm.

3.2. Transport properties

All films were prepared on a thin flexible polyimide substrate with a thickness of ~10 μm. As it was mentioned above, the advantage of the polyimide substrate is its low thermal conductivity ($\kappa \approx 3.5 \times 10^{-3}$ W/cm K at $T = 300$ K), excellent thermal stability in the air, solvent

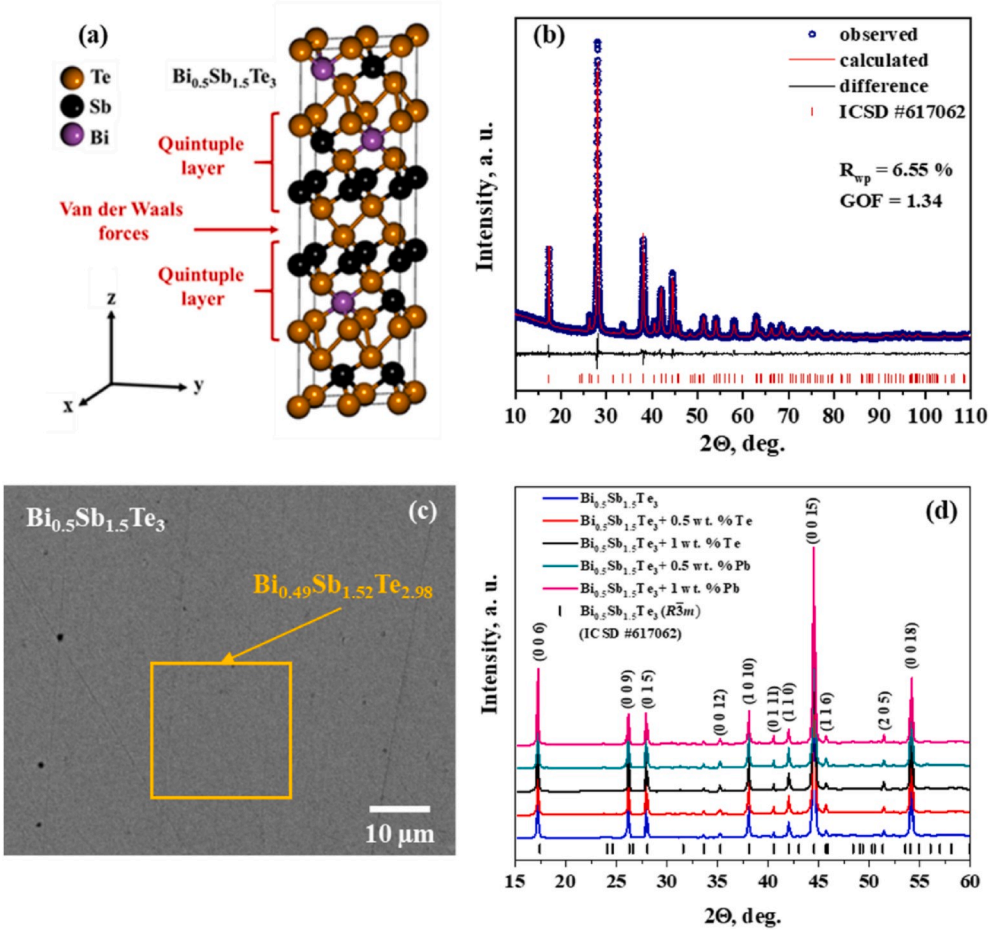

Fig. 1. (a) Crystal structure of $Bi_{0.5}Sb_{1.5}Te_3$. (b) Refined powder XRD pattern of as cast $Bi_{0.5}Sb_{1.5}Te_3$ sample. (c) SEM image with the EDS elemental analyses of polished surface of $Bi_{0.5}Sb_{1.5}Te_3$ specimen after synthesis. (d) XRD patterns of $Bi_{0.5}Sb_{1.5}Te_3$-based films on a polyimide substrate.

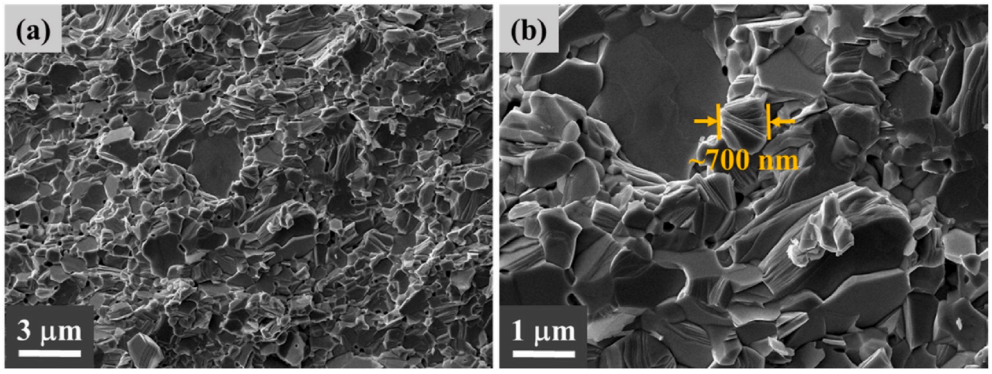

Fig. 2. Secondary emission images for representative $Bi_{1.5}Sb_{0.5}Te_3$ film on a polyimide substrate with (a) lower and (b) higher resolution.

resistance, as well as mechanical and electrical properties acceptable for module fabrication [33,34]. Moreover, using a flexible substrate for the preparation of film thermoelectrical modules (FTEM) opens new horizons for their applications.

Fig. 3(a–d) shows the results of studies of transport properties of *p*-$Bi_{0.5}Sb_{1.5}Te_3$ films of different composition: $Bi_{0.5}Sb_{1.5}Te_3$ + 1.0 wt % Te, $Bi_{0.5}Sb_{1.5}Te_3$ + 0.5 wt % Te, $Bi_{0.5}Sb_{1.5}Te_3$, $Bi_{0.5}Sb_{1.5}Te_3$ + 0.5 wt % Te_3 and $Bi_{0.5}Sb_{1.5}Te_3$ + 1 wt % Pb, with a thickness of 3 ± 0.5 μm on a flexible polyimide substrate.

For obtaining the charge carrier concentration as a function of temperature for the investigated film, Hall effect was measured over the temperature range of 80–400 K. Fig. 3(a) shows the measurement results. The films show positive values of the Hall coefficient over the entire investigated temperature range. This result is related to hole conductivity (*p*-type) in $Bi_{0.5}Sb_{1.5}Te_3$-based films. Samples with over stochiometric Te show almost linear behavior of the Hall constant R_H over the investigated temperature range. The values of Hall constant R_H decrease slightly with increasing temperature for samples with over stoichiometric Pb.

Fig. 3(b) shows the Seebeck coefficient *S* for *p*-$Bi_{0.5}Sb_{1.5}Te_3$ films as a function of temperature. The Seebeck coefficient for *p*-$Bi_{0.5}Sb_{1.5}Te_3$ films has positive values over the investigated temperature range, which is typical for semiconductors with hole-type conductivity. The absolute value of the Seebeck coefficient for $Bi_{0.5}Sb_{1.5}Te_3$ with over stochiometric Pb increases over a wide temperature range of 80–400 K. The effect of the minority carriers is absent due to the high concentration of carriers in these films. The stochiometric $Bi_{0.5}Sb_{1.5}Te_3$ film and films with over stochiometric Te reach the maximum Seebeck coefficient, and then start to decrease due to the effect of minority carriers.

The temperature trends of the electrical conductivity σ for *p*-$Bi_{0.5}Sb_{1.5}Te_3$ films are shown in Fig. 3(c). The value of σ increases with the growth of the carrier concentration *p* over the investigated temperature range. The temperature dependencies of σ for *p*-$Bi_{0.5}Sb_{1.5}Te_3$ films show a decreasing tendency, which indicates metallic behavior.

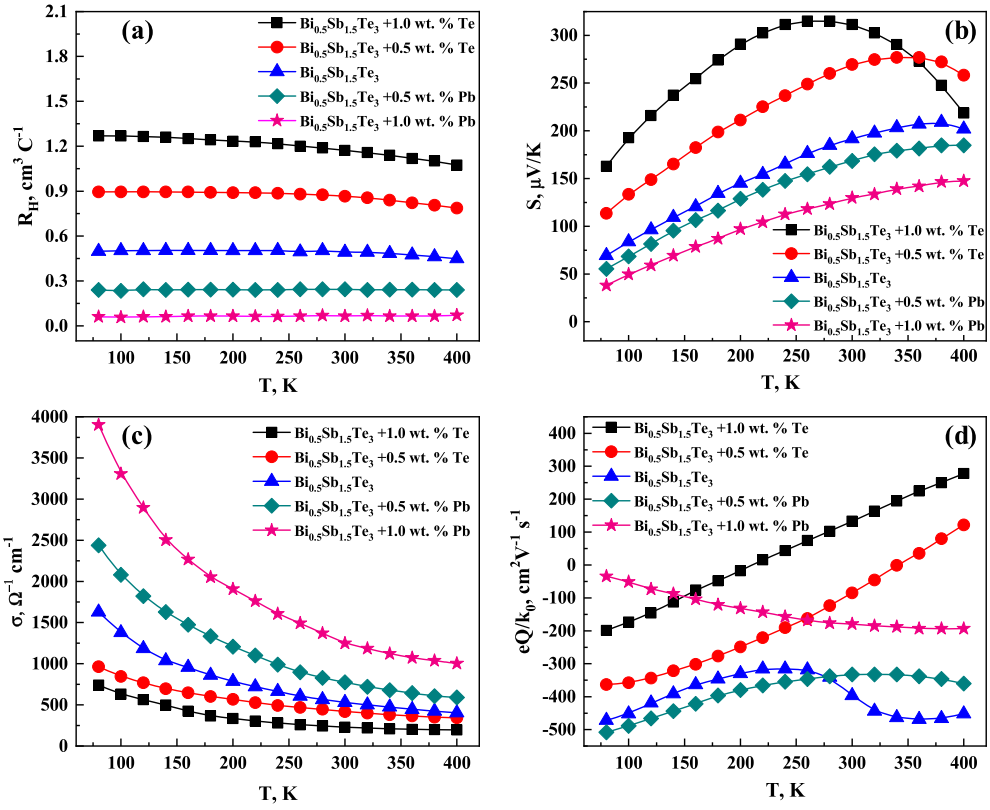

Fig. 3. Hall coefficient R_H (a), Seebeck coefficient *S* (b), electrical conductivity (c), and transverse Nernst coefficient *Q* (d) as a function of temperature for *p*-$Bi_{0.5}Sb_{1.5}Te_3$ films.

Before analyzing the Nernst coefficient measurements made for *p*-$Bi_{0.5}Sb_{1.5}Te_3$ films, the particular importance of this effect should be discussed. The Hall effect is a measure of the deflection of the drift carriers in a magnetic field. The Nernst effect is similar to the Hall effect except that the carriers are driven by a temperature gradient rather than the applied deflection. Carriers originating from the hot end of the sample would have higher energy and velocity compared to carriers from the cold end. The magnetic field will deflect the slower-moving carriers into a shorter-radius orbit than the faster-moving carriers and create a Nernst electric field.

For a parabolic model and charge carrier mean free path represented as $l = l_0E^r$, where l_o is the constant, E is the charge carrier energy, and r is the scattering parameter (equal to 0)), the Nernst coefficient is determined by Ref. [25]:

$$\frac{Q}{(k_0/e)} = \frac{\left(2r+\frac{3}{2}\right)F_{2r+\frac{3}{2}}(\mu^*)}{\left(2r+\frac{1}{2}\right)F_{2r-\frac{1}{2}}(\mu^*)} - \frac{(r+2)F_{r+1}(\mu^*)}{(r+1)F_r(\mu^*)}, \quad (4)$$

where k_0 is the Boltzmann constant, e is the electron charge, $F(\mu^*)$ are Fermi-Dirac integrals. The parameter $\mu^* = (E_F - E_V)/k_oT$ is the reduced Fermi energy, where E_V is the valence-band maximum, and E_F is the Fermi level, T is the absolute temperature. According to eq. (4) Q depends only on the carrier scattering mechanism (parameter r) and the location of Fermi level E_F. In contrast to the Hall coefficient, the sign of the Nernst coefficient does not depend on the charge carrier sign.

The presence of minority carriers in transport leads to a decrease of the Hall coefficient, as well as the Seebeck coefficient, and for intrinsic area these coefficients are close to zero. In the beginning of the intrinsic conduction (two types of carriers: electrons and holes), the Nernst coefficient sharply increases with possible sign change. For this reason, the Nernst coefficient is the most sensitive to the beginning of the intrinsic regime.

Fig. 3(d) demonstrates the temperature trends of the Nernst coefficient Q over the investigated temperature range of 80–400 K for *p*-$Bi_{0.5}Sb_{1.5}Te_3$ films. The Q parameter for $Bi_{0.5}Sb_{1.5}Te_3$ samples with over stoichiometric Te increases over the entire temperature range, indicating the presence of minority carriers in transport. This observation is also consistent with the $S(T)$ maximum for these films, which is also an indication of the beginning of the intrinsic regime.

3.3. Scattering parameter and density of states effective mass

The fundamental parameters for the analysis of the transport properties, as well as the thermoelectric performance of semiconductors are the effective mass m^* and the scattering coefficient r. Based on the four-coefficients method, we performed a direct assessment of the effective mass and carrier scattering mechanism for *p*-$Bi_{0.5}Sb_{1.5}Te_3$ films. For a single parabolic band, the Seebeck coefficient S is defined as [35]:

$$S = \frac{k_0}{e}\left[\frac{(r+2)F_{r+1}(\mu^*)}{(r+1)F_r(\mu^*)} - \mu^*\right], \quad (5)$$

In a strong magnetic field, the Seebeck coefficient S is isotropic, i.e. it does not depend on the scattering mechanism, and is a function of the reduced chemical potential:

$$S = \frac{k_0}{e}\left[\frac{5F_{5/2}(\mu^*)}{3F_{1/2}(\mu^*)} - \mu^*\right]. \quad (6)$$

The density of states effective mass m^* and the scattering parameter r can be directly determined from a set of four kinetic coefficients S, σ, R_H and Q using the following equations [25,36]:

$$m^* = \left(\frac{3n}{\pi}\right)^{2/3}\frac{e\hbar^2}{k_0^2T}\left(S - \frac{Q}{|R|\sigma}\right), \quad (7)$$

$$r = \frac{Q/|R|\sigma}{S - Q/|R|\sigma}. \quad (8)$$

The results of the estimation of m^* and r for *p*-$Bi_{0.5}Sb_{1.5}Te_3$ films at 100 K are shown in Table 1. For all films at the given temperature the scattering parameter r is close to ≈0, which indicates acoustic phonons as the main scattering mechanism in the investigated films [24]. Scattering on acoustic phonons is also typical for high-performance bulk *p*-$Bi_{0.5}Sb_{1.5}Te_3$ samples. The m_d values calculated using data of S, Q, R, and σ for *p*-$Bi_{0.5}Sb_{1.5}Te_3$ films at 100 K decrease slightly from 0.5 to 0.6 with increasing concentration p (Table 1).

The Hall concentrations of the investigated films are changing from 4.9×10^{18} cm^{-3} to 1.1×10^{20} cm^{-3} in accordance with the nominal composition of the films. The over stochiometric Te reduces the carrier concentration, while doping with Pb increases the carrier concentration of $Bi_{0.5}Sb_{1.5}Te_3$ films. The mobility μ of *p*-$Bi_{0.5}Sb_{1.5}Te_3$ films is within the range of 200–800 cm $^2V^{-1}s^{-1}$, which is comparable to the values for *p*-$Bi_{0.5}Sb_{1.5}Te_3$ bulk specimens [23,24].

3.4. Thermoelectric properties

Table 2 demonstrates the measured thermoelectric properties (the Seebeck coefficient S, electrical conductivity σ and thermal conductivity κ) at $T = 300$ K for three *p*-$Bi_{0.5}Sb_{1.5}Te_3$ films on a flexible polyimide substrate. For comparison, thermoelectric parameters of bulk $Bi_{0.5}Sb_{1.5}Te_3$ specimens from Ref. [23,24] are also given in Table 2. The calculated thermoelectric figure of merit Z for $Bi_{0.5}Sb_{1.5}Te_3$ + 0.5 wt % Te film achieves the value $Z \approx 3.0 \times 10^{-3}$ K^{-1} at 300 K, which is practically equal to Z value for *p*-$Bi_{0.5}Sb_{1.5}Te_3$ bulk samples. The estimated lattice thermal conductivity κ_L (details of the calculation of κ_L are given below) values at 300 K are equal to 8.1–10 W/cm K for $Bi_{0.5}Sb_{1.5}Te_3$ films. We do not observe an atypical decrease in the lattice thermal conductivity due to scattering on the grain boundaries because the heat transport in the investigated films is mostly defined by short-range acoustic phonons. This is due to the shorter mean free path of the phonon propagation for the $Bi_{0.5}Sb_{1.5}Te_3$ solid solution in comparison with the size of grains of the investigated films. High thermoelectric performance of the studied films is associated with the enhanced Seebeck coefficient S and is similar to the bulk crystal values of the lattice thermal conductivity κ_L.

Fig. 4(a) shows the power factor $PF = S^2\sigma$ for *p*-$Bi_{0.5}Sb_{1.5}Te_3$ films. Typically, samples with over stochiometric Te represent high value of PF up to ~30 μV cm^{-1} K^{-2} at 200 K and 300 K, respectively, due to the optimal position of the Fermi level (close to the top of the valence band [7]). The absolute value of the power factor for $Bi_{0.5}Sb_{1.5}Te_3$ + 0.5 wt % Te film is above ~25 μV $cm^{-1}K^{-2}$ over the entire temperature range of 200–400 K. The power factor for the best fabricated *p*-$Bi_{0.5}Sb_{1.5}Te_3$ films with 0.5–1.0 wt % Te in comparison with the literature data with relatively similar carrier concentration is shown in Fig. 4(b). Besides excellent thermoelectric performance, the advantages of the developed films are high flexibility due to a thin polyimide substrate. The obtained value of PF is also higher compared to $Bi_{0.5}Sb_{1.5}Te_3$ film on a polyimide substrate recently reported by Shang et al. [32]. The possible reason for this improvement of PF in our work could be explained by a narrower polyimide substrate (~10 μm), attuned carrier concentration, as well as

Table 1
Carrier concentration p, carrier mobility μ, effective mass m^*/m_0 and scattering parameter r for *p*-$Bi_{0.5}Sb_{1.5}Te_3$-based films at 100 K.

Sample composition	p, cm^{-3}	μ, $cm^2V^{-1}s^{-1}$	m^*/m_0	r
$Bi_{0.5}Sb_{1.5}Te_3$ + 1.0 wt % Te	4.9×10^{18}	8.01×10^2	0.50	0.2
$Bi_{0.5}Sb_{1.5}Te_3$ + 0.5 wt % Te	7.0×10^{18}	7.56×10^2	0.52	0.2
$Bi_{0.5}Sb_{1.5}Te_3$	1.2×10^{19}	6.93×10^2	0.55	0.2
$Bi_{0.5}Sb_{1.5}Te_3$ + 0.5 wt % Pb	2.7×10^{19}	4.87×10^2	0.58	0.1
$Bi_{0.5}Sb_{1.5}Te_3$ + 1.0 wt % Pb	1.1×10^{20}	1.90×10^2	0.60	0

Table 2
Thermoelectric properties of p-$Bi_{0.5}Sb_{1.5}Te_3$ films and bulk crystals at $T = 300$ K.

Composition	Type of material	Seebeck coefficient S, μV/K	Electrical conductivity σ, $\Omega^{-1}cm^{-1}$	Thermal conductivity κ, W/cm K	Lattice thermal conductivity κ_{lat}, W/cm K	Figure of merit $Z \times 10^3$, K^{-1}	Ref.
$Bi_{0.5}Sb_{1.5}Te_3$ + 1.0 wt % Te	film	310	230	9.3	8.1	2.4	This work
$Bi_{0.5}Sb_{1.5}Te_3$ + 0.5 wt % Te	film	270	420	10.0	8.3	3.0	This work
$Bi_{0.5}Sb_{1.5}Te_3$ + 0.5 wt % Pb	film	170	775	11.7	8.2	1.9	This work
$Bi_{0.5}Sb_{1.5}Te_3$	bulk	200	1150	15.5	10.0	3.0	[23]
$Bi_{0.5}Sb_{1.5}Te_3$	bulk	205	1020	14.5	9.9	2.9	[24]

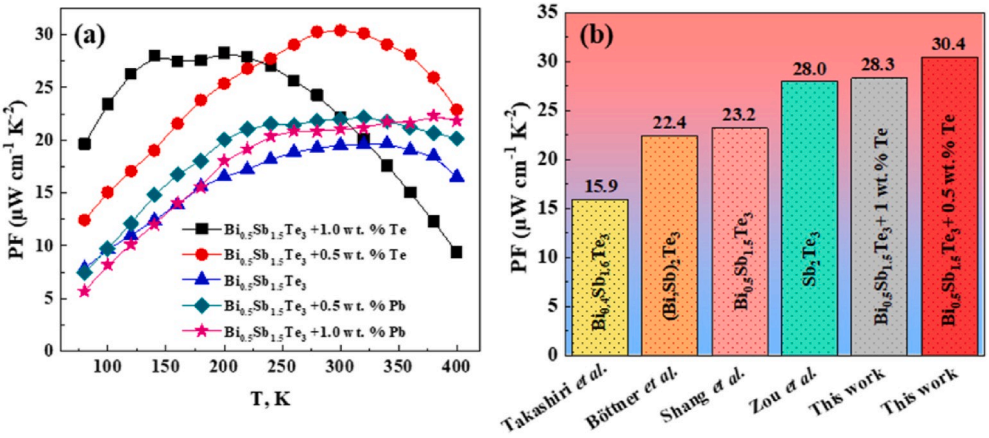

Fig. 4. (a) Power factor as a function of temperature for p-$Bi_{0.5}Sb_{1.5}Te_3$ films. (b) Comparison of the power factor for several high-performance p-type $(Bi,Sb)_2Te_3$-based films [14,20,32,37].

optimized annealing conditions.

Heat transport is determined by the total thermal conductivity κ of a semiconductor, which consists of three components: the lattice thermal conductivity of phonons κ_L, the electronic thermal conductivity of free carriers κ_e and the ambipolar thermal conductivity of electron-hole pairs κ_a in the intrinsic conduction region [24]:

$$\kappa = \kappa_L + \kappa_e + \kappa_a \ . \tag{9}$$

For one type of carriers (holes) in the majority area, only the first two coefficients of thermal conductivity influence the value of κ. The value of the total thermal conductivity as a function of temperature was calculated by summing up the lattice and the electronic thermal conductivity.

The lattice thermal conductivity at $T = 300$ K was estimated from the direct measurement of the thermal diffusivity and is shown in Table 2. The lattice thermal conductivity as a function of temperature was assumed to be similar to the bulk material [7]. The values of κ_e have been obtained using Wiedemann-Franz law:

$$\kappa_e = L_0 \sigma T \ , \tag{10}$$

where L is the Lorentz number, which can be calculated using the following equation [24]:

$$L = \left(\frac{k_0}{e}\right)^2 \left[3\frac{F_2(\mu^*)}{F_0(\mu^*)} - \left(2\frac{F_2(\mu^*)}{F_0(\mu^*)}\right)^2\right]. \tag{11}$$

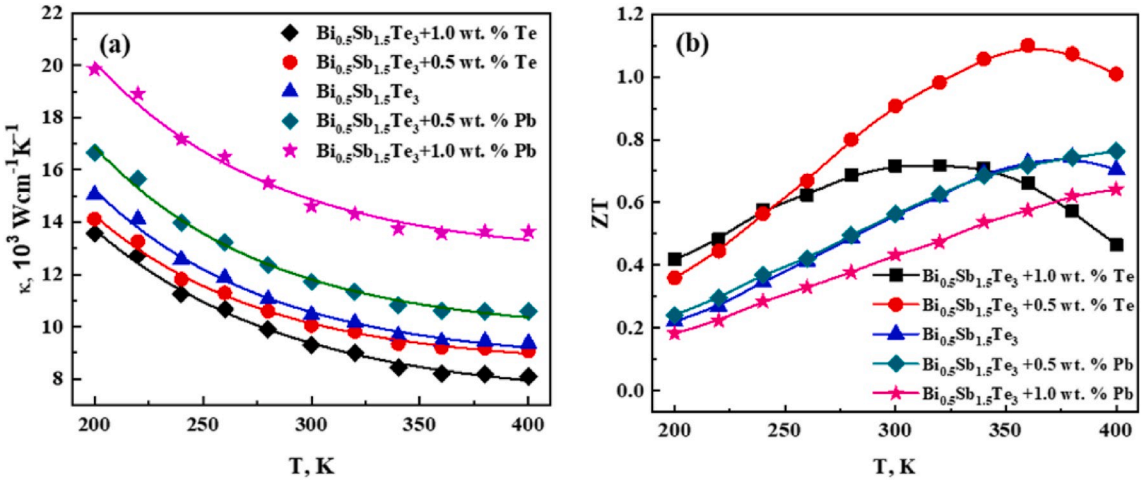

Fig. 5. Total thermal conductivity κ (a) and dimensionless thermoelectric figure of merit ZT (b) as a function of temperature for p-$Bi_{0.5}Sb_{1.5}Te_3$ films.

At the acoustic phonon scattering of charge carriers, the reduced Fermi energy μ* can be obtained by fitting the Seebeck coefficient using equation (5).

Fig. 5(a) shows the temperature dependent thermal conductivity for the investigated $Bi_{0.5}Sb_{1.5}Te_3$ films. The values of κ for the investigated samples decrease over the investigated temperature range of 200–400 K. In contrast to the Nernst and Seebeck coefficients, the intrinsic regime was not detected from the temperature trends of electrical and thermal conductivity.

Fig. 5(b) shows the temperature dependence of the dimensionless thermoelectric figure of merit *ZT* for *p*-$Bi_{0.5}Sb_{1.5}Te_3$ films in the temperature range from 200 to 400 K. The maximum *ZT* value has reached the value of ~1.1 for $Bi_{0.5}Sb_{1.5}Te_3$ + 0.5 at. % Te film, which is comparable with the *ZT* parameter for the best sample of the extruded *p*-$Bi_{0.5}Sb_{1.5}Te_3$ bulk material [7]. Such a promising value clearly shows that *p*-$Bi_{0.5}Sb_{1.5}Te_3$ films could be an excellent candidate for microscale applications.

4. Conclusions

The *p*-type $Bi_{0.5}Sb_{1.5}Te_3$-based films with an optimal carrier concentration have been prepared by a flash evaporation method. The technological parameters for the fabrication of *p*-$Bi_{0.5}Sb_{1.5}Te_3$ films on a thin flexible (polyimide) substrate have been optimized to maximize thermoelectric performance.

A systematic study of the transport properties (the Hall coefficient, the Seebeck coefficient, electrical conductivity, transverse Nernst coefficient) have been carried out over the entire temperature range of 80–400 K for *p*-$Bi_{0.5}Sb_{1.5}Te_3$ films. Based on the four-coefficients method, the density of states effective mass and carrier scattering mechanism were estimated.

The power factor for $Bi_{0.5}Sb_{1.5}Te_3$ + 0.5 at. % Te film reaches a value of ~30 μW cm^{-1} K^{-2} at T = 300 K, which is among the highest values of the PF for a film on a thin flexible polyimide substrate reported in the literature.

Direct measurement of thermal diffusivity along the film allowed an accurate assessment of the thermoelectric figure of merit for film samples on a flexible substrate with the consideration of the anisotropic effect of Bi_2Te_3-based materials. The achieved value of $Z = 3.0 \times 10^{-3}$ K^{-1} at 300 K for $Bi_{0.5}Sb_{1.5}Te_3$ + 0.5 wt % Te film is state-of-the-art, even when compared to bulk materials.

The significant enhancement of thermoelectric performance of *p*-$Bi_{0.5}Sb_{1.5}Te$ films on a flexible substrate opens up new horizons for the fabrication of Film Thermoelectric Modules (FTEM), which could be an excellent candidate for application in micro-scale Thermoelectric Generators (TEG).

Declaration of competing interest

The authors declare that they have no known competing financial interests or personal relationships that could have appeared to influence the work reported in this paper.

CRediT authorship contribution statement

T. Parashchuk: Investigation, Visualization, Writing - original draft. **O. Kostyuk:** Formal analysis, Data curation. **L. Nykyruy:** Software, Writing - review & editing. **Z. Dashevsky:** Methodology, Writing - review & editing, Supervision.

Acknowledgments

This research was supported by the Ministry of Education and Science of Ukraine for young scientists "Technology of thin-film thermoelectric micromodules based on multicomponent compounds with quantum-size effects" (state registration number 0119U100062). T.P. acknowledges support by Foundation for Polish Science under TEAM-TECH/2016-2/14 Grant.

Appendix. Film preparation by a flash evaporation method

A set up for obtaining films by flash evaporation method is shown in Fig. 6. For film preparation, $Bi_{0.5}Sb_{1.5}Te_3$ powder was introduced into the preheated quartz crossable 1 from a mechanically vibrated powder vessel 7. The evaporator is a quartz crossable 1 with a heater 2, surrounded by a molybdenum heat screen 3. The powdered material is introduced to the crucible from the powder vessel 7 through a water-cooled channel 6. The delivery of powder is realized by shaking the powder vessel 7 with an eccentric. The heating of the substrate is received by substrate heater 5. All parts of the device are located in chamber 8 under a vacuum of 10^{-5} mbar.

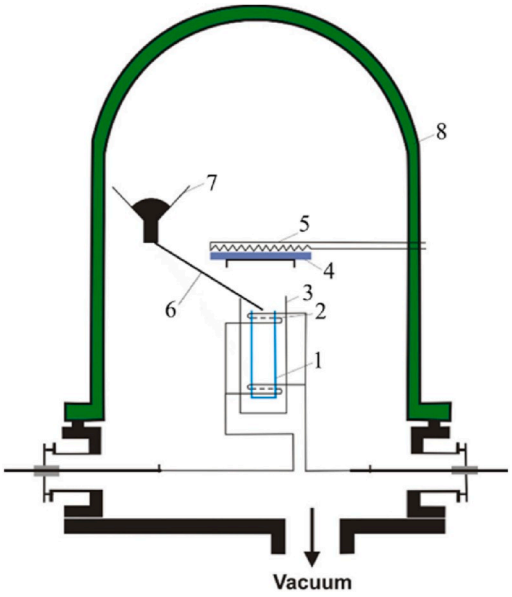

Fig. 6. Schematic view of flash evaporation. 1 - quartz crucible, 2 - crucible heater, 3 - heat shield, 4 - substrate, 5 - substrate heater, 6 - channel, 7-powder vessel, 8 - vacuum chamber.

References

[1] A.P. Goncalves, C. Godart, Alternative strategies for thermoelectric materials development, in: V. Zlatic, A. Hewson (Eds.), New Materials for Thermoelectric Applications: Theory and Experiment, Springer, New York, 2013, pp. 1–24.

[2] D.M. Rowe, Thermoelectric Handbook, Macro to Nano, CRC Press, Boca Raton, 2005.

[3] K. Tappura, Kaarle Jaakkola, A thin-film thermoelectric generator for large-area applications, Proceedings 2 (13) (2018) 779.

[4] K. Settaluri, H. Lo, R.J. Ram, Thin thermoelectric generator system for body energy harvesting, J. Electron. Mater. 41 (2017) 984–988.

[5] R. Venkatasubramanian, E. Siivola, T. Colpitts, B. O'Quinn, Thin-film thermoelectric devices with high room-temperature figures of merit, Nature 413 (2001) 597–602.

[6] P. Fan, Z. Zheng, Z. Cai, T. Chen, P. Liu, The high performance of a thin film thermoelectric generator with heat flow running parallel to film surface, Appl. Phys. Lett. 102 (2013), 033904.

[7] Z. Dashevsky, S. Skipidarov, Investigating the performance of bismuth - antimony telluride in novel materials and device design concepts, in: M. Nikitin, S. Skipidarov (Eds.), Novel Thermoelectric Materials and Device Design Concepts, Springer, New York, 2019, pp. 3–23.

[8] B.M. Goltsman, B.A. Kudinov, I.A. Smirnov, Semiconductor Thermoelectric Materials Based on Bi_2Te_3, Nauka, Moskow, 1972 (In Russian).

[9] J. Herremans, B. Wiendliocha, Tetradymites: Bi_2Te_3-related materials, in: C. Uher (Ed.), Materials Aspect of Thermoelectricity, CRS Press, Boca Raton, 2016, pp. 39–94.

[10] O. Ben-Yehuda, R. Shuker, Y. Gelbstein, Z. Dashevsky, M.P. Dariel, Highly textured Bi_2Te_3-based materials for thermoelectric energy conversion, J. Appl. Phys. 101 (2007) 113707.

[11] L.M. Goncalves, C. Couto, P. Alpuim, A.G. Rolo, F. Völklein, J.H. Correia, Optimization of thermoelectric properties on Bi_2Te_3 thin films deposited by thermal co-evaporation, Thin Solid Films 518 (2010) 2816–2821.

[12] X. Duan, Y. Jiang, Annealing effects on the structural and electrical transport properties of n-type $Bi_2Te_{2.7}Se_{0.3}$ thin films deposited by flash evaporation, Appl. Surf. Sci. 256 (2010) 7365–7370.

[13] L.W. da Silva, M. Kaviany, C. Uher, Thermoelectric performance of films in the bismuth-tellurium and antimony-tellurium systems, J. Appl. Phys. 97 (2005) 114903.

[14] M. Takashiri, T. Shirakawa, K. Miyazaki, H. Tsukamoto, Fabrication and characterization of bismuth–telluride-based alloy thin film thermoelectric generators by flash evaporation method, Sens. Actuat. A Phys. 138 (2007) 329–334.

[15] G. Wang, L. Endicott, C. Uher, Structure and transport properties of Bi_2Te_3 films, Sci. Adv. Mater. 3 (2011) 73–98.

[16] E. Symeou, M. Pervolaraki, C.N. Mihailescu, G.I. Athanasopoulos, C. Papageorgiou, T. Kyratsi, J. Giapintzakis, Thermoelectric properties of $Bi_{0.5}Sb_{1.5}Te_3$ thin films grown by pulsed laser deposition, Appl. Surf. Sci. 336 (2015) 138–142.

[17] P. Fan, Z.-H. Zheng, Z.-K. Cai, T.-B. Chen, P.-J. Liu, X.-M. Cai, D.-P. Zhang, G.-X. Liang, J.-T. Luo, The high performance of a thin film thermoelectric generator with heat flow running parallel to film surface, Appl. Phys. Lett. 102 (2013), 033904.

[18] D. Bourgault, C.G. Garampon, N. Caillault, L. Carbone, J.A. Aymami, Thermoelectric properties of n-type $Bi_2Te_{2.7}Se_{0.3}$ and p-type $Bi_{0.5}Sb_{1.5}Te_3$ thin films deposited by direct current magnetron sputtering, Thin Solid Films 516 (2008) 8579–8583.

[19] H. Obara, S. Higomo, M. Ohta, A. Yamoroto, K. Ueno, T. Iida, Thermoelectric properties of Bi_2Te_3-based thin films with fine grains fabricated by pulsed laser deposition, Jpn. J. Appl. Phys. 48 (2009), 085506.

[20] H. Zou, D.M. Rowe, S.G.K. Williams, Peltier effect in a co-evaporated Sb_2Te_3(P)-Bi_2Te_3(N) thin film thermocouple, Thin Solid Films 408 (2002) 270–274.

[21] H.-J. Wu, W.-T. Yen, High thermoelectric performance in Cu-doped Bi2Te3 with carrier-type transition, Acta Mater. 157 (2018) 33.

[22] R. Deng, X. Su, S. Hao, Z. Zheng, M. Zhang, H. Xie, W. Liu, Y. Yan, C. Wolverton, C. Uher, M.G. Kanatzidis, X. Tang, High thermoelectric performance in $Bi_{0.46}Sb_{1.54}Te_3$ nanostructured with ZnTe, Energy Environ. Sci. 6 (2018) 1520.

[23] Z.M. Dashevsky, P.P. Konstantinov, S.Ya Skipidarov, New direction in the application of thermoelectric energy converters, Semiconductors 53 (2019) 861–864.

[24] L.D. Ivanova, L.I. Petrova, JuV. Hranatkina, V.B. Sokolov, S.Ja Skipidarov, N. I. Duvankov, Extruded materials for thermoelectric coolers, Inorg. Mater. 44 (2008) 687–691.

[25] B.M. Goltzman, Z.M. Dashevsky, V.I. Kaydanov, N.V. Kolomoetz, Film Thermoelements: Physics and Application, Nauka, Moscow, 1985 (in Russian).

[26] B. Dzundza, L. Nykyruy, T. Parashchuk, E. Ivakin, Y. Yavorsky, L. Chernyak, Z. Dashevsky, Transport and thermoelectric performance of n-type PbTe films, Phys. B Condens. Matter (2020) 412178.

[27] E.V. Ivakin, I.G. Kisialiou, L.I. Nykyruy, Y.S. Yavorskyy, Optical studies of heat transfer in PbTe:Bi(Sb) thin films, Semiconductors 52 (2018) 1691–1695.

[28] S. Lee, K. Esfarjani, T. Luo, J. Zhou, Z. Tian, G. Chen, Resonant bonding leads to low lattice thermal conductivity, Nat. Commun. 5 (2014) 3525.

[29] X. He, D.J. Singh, P. Boon-On, M.W. Lee, L. Zhang, Dielectric behavior as a screen in rational searches for electronic materials: metal pnictide sulfosalts, J. Am. Chem. Soc. 140 (2018) 18058–18065.

[30] X. Mu, H. Zhou, D. He, W. Zhao, P. Wei, W. Zhu, X. Nie, H. Liu, Q. Zhang, Enhanced electrical properties of stoichiometric $Bi_{0.5}Sb_{1.5}Te_3$ film with high-crystallinity via layer-by-layer in-situ Growth, Nano Energy 33 (2017) 55–64.

[31] C.V. Manzano, B. Abad, M. Munoz Rojo, Y.R. Koh, S.L. Hodson, A.M. Lopez Martinez, X. Xu, A. Shakouri, T.D. Sands, T. Borca-Tasciuc, M. Martin-Gonzalez, Anisotropic effects on the thermoelectric properties of highly oriented electrodeposited Bi_2Te_3 films, Sci. Rep. 6 (2016) 19129.

[32] H. Shang, C. Dun, Y. Deng, T. Li, Z. Gao, L. Xiao, H. Gu, D.J. Singh, Z. Ren, F. Ding, $Bi_{0.5}Sb_{1.5}Te_3$-based films for flexible thermoelectric devices, J. Mater. Chem. A 8 (2020) 4552–4561.

[33] Pei-Ju Chen, Chien-Neng Lian, Thermoelectric transport properties of Bi–Te based thin films on strained polyimide substrates, Appl. Phys. Lett. 105 (2014) 133903.

[34] Soo-Jin Park, Ki-Sook Cho, Sung-Hyun Kim, A study on dielectric characteristics of fluorinated polyimide thin film, J. Colloid Interface Sci. 272 (2004) 384–390.

[35] T. Parashchuk, Z. Dashevsky, K. Wojciechowski, Feasibility of a high stable PbTe:In semiconductor for thermoelectric energy applications, J. Appl. Phys. 125 (2019) 245103.
[36] D.L. Young, T.J. Coutts, V.I. Kaydanov, Density-of-states effective mass and scattering parameter measurements by transport phenomena in thin films, Rev. Sci. Instrum. 71 (2000) 462–466.
[37] H. Bottner, J. Nunus, A. Gavrikov, G. Kühner, M. Jägle, C. Künzel, D. Eberhard, G. Plescher, A. Schubert, K.-H. Schlereth, New thermoelectric components using microsystem technologies, J. Microelectromech. Syst. 13 (3) (2004) 414–420.